S-matrix calculations of energy levels of sodiumlike ions

J. Sapirstein*
University of Notre Dame, Notre Dame, Indiana 46556, USA

K. T. Cheng (鄭國錚)†
Lawrence Livermore National Laboratory, Livermore, California 94550, USA

(Received 19 May 2015; published 24 June 2015)

A recent *S*-matrix-based QED calculation of energy levels of the lithium isoelectronic sequence is extended to the general case of a valence electron outside an arbitrary filled core. Emphasis is placed on modifications of the lithiumlike formulas required because more than one core state is present, and an unusual feature of the two-photon exchange contribution involving autoionizing states is discussed. The method is illustrated with a calculation of the energy levels of sodiumlike ions, with results for $3s_{1/2}$, $3p_{1/2}$, and $3p_{3/2}$ energies tabulated for the range $Z = 30$–100. Comparison with experiment and other calculations is given, and prospects for extension of the method to ions with more complex electronic structure discussed.

DOI: 10.1103/PhysRevA.91.062508 PACS number(s): 12.20.Ds

I. INTRODUCTION

Quantum electrodynamics (QED), the relativistic field theory of the electromagnetic interaction of charged particles, describes the simplest atom, hydrogen, with high accuracy. This accuracy of both experiment and theory is continuously improving, with the level of parts per billion (ppb) not unusual for both [1]. To achieve agreement between theory and experiment, QED effects, most prominently the one-loop radiative correction known as the Lamb shift, must of course be included.

The definition of a QED effect is particularly straightforward for hydrogen, simply being any correction to the analytically known energy levels predicted by the Dirac equation. If the nucleus is treated as an infinitely heavy point charge, a modification of the interaction picture of QED introduced by Furry [2] gives a framework for calculating QED effects. In particular, the Lamb shift is a precisely defined quantity involving the propagator of an electron in the field of the point charge. For example, before regularization and renormalization, the self-energy part of the one-loop Lamb shift of an electron in state v when the nuclear charge is $Z|e|$ is

$$E_v(\mathrm{SE}) = -ie^2 \int d^3x\, d^3y \int \frac{d^4k}{(2\pi)^4} \frac{e^{i\vec{k}\cdot(\vec{x}-\vec{y})}}{k^2 + i\delta} \times \bar{\psi}_v(\vec{x})\gamma_\mu S_F(\vec{x},\vec{y};\epsilon_v - k_0)\gamma^\mu \psi_v(\vec{y}), \quad (1)$$

with the electron propagator obeying the equation

$$\left[\left(E + \frac{Z\alpha}{r}\right)\gamma_0 + i\vec{\gamma}\cdot\vec{\nabla}_x - m\right] S_F(\vec{x},\vec{y};E) = \delta^3(\vec{x}-\vec{y}). \quad (2)$$

Advances in numerical methods have led to its evaluation accurate to under 1 Hz [3].

However, as soon as more than one electron is present, the definition of a QED effect is less obvious, as one no longer has either an analytically or a numerically known analog to the Dirac energy levels. If one allows the definition of QED effects to include relativistic corrections, one approach is to define the energy relative to which a QED effect is defined as E_S, the solution of the Schrödinger equation $H\Psi = E_S\Psi$ for N electrons, with Hamiltonian

$$H = \sum_{i=1}^{N}\left[\frac{\vec{p}_i^{\,2}}{2m} - \frac{Z\alpha}{r_i}\right] + \sum_{i<j}\frac{\alpha}{|\vec{r}_i - \vec{r}_j|}. \quad (3)$$

Effective field theory methods, introduced as nonrelativistic QED (NRQED by Caswell and Lepage [4], provide a systematic method of including corrections to E_S from QED effects. When considering few-electron atoms and molecules, variational methods allow E_S to be determined very precisely. The ground-state energy of helium is a striking example [5],

$$E_S = -2.903\,724\,377\,034\,119\,598\,311\ldots \quad (4)$$

in atomic units, with many more digits not shown. The QED corrections, while challenging to calculate, are basically under control at the same level as for hydrogen. Examples of state-of-the-art calculations are the fine structure of helium [6] and the hydrogen molecule [7].

When variational methods become impractical, a mean central field $U(r)$ is introduced, and the Hamiltonian is reorganized to $H = H_0 + V$, with

$$H_0 = \sum_{i=1}^{N}\left[\frac{\vec{p}_i^{\,2}}{2m} - \frac{Z\alpha}{r_i} + U(r_i)\right] \quad (5)$$

and

$$V = \sum_{i<j}\frac{\alpha}{|\vec{r}_i - \vec{r}_j|} - \sum_i U(r_i). \quad (6)$$

The Rayleigh-Schrödinger perturbation expansion in V is known as many-body perturbation theory (MBPT) and will have a close relation to the QED approach we use.

In this paper we treat highly charged ions with many electrons. In these ions, relativistic effects are too large to be included perturbatively, and there are too many electrons to allow the use of variational methods, so an approach along the

*jsapirst@nd.edu
†ktcheng@llnl.gov

lines of MBPT is called for. A relativistic form of MBPT can be introduced by replacing the nonrelativistic kinetic energy $\vec{p}_i^{\,2}/2m$ with $\vec{\alpha}_i \cdot \vec{p}_i + \beta_i m$ in Eq. (5). While there are well-known problems present when carrying out the sums over intermediate states of MBPT when negative energy states are involved [8,9], they can be avoided by simply excluding those states from those summations. E_D, a relativistic generalization of E_S, can then be defined.

When $U(r)$ is chosen to be the Hartree-Fock potential, sets of calculations of E_D have been carried out up to third order in MBPT for the lithiumlike [10], sodiumlike [11], and copperlike [12] isoelectronic sequences. Significant discrepancies with experiment are found in all cases, as expected because QED effects are not included in E_D. A useful approximate inclusion of the leading QED effect, the Lamb shift, for the three sequences was given in Ref. [13]. However, a QED approach equal in rigor to NRQED can be applied, based on a modification of the Furry representation [2] used in hydrogen calculations. An early application of this approach was given by Blundell [14], and more recently two calculations of the lithiumlike sequence have been carried out [15,16]. We note also another approach to incorporating QED into the many-body problem by Lindgren [17].

Furry representation changes the interaction picture, where electrons propagate freely, in such a way that the electrons propagate in an external Coulomb field, as described in Eq. (2). The unitary transformation that does this is easily modified to incorporate the mean central potential $U(r)$, although we have to use local approximations to the original Hartree-Fock potential because of its nonlocality. Just as with hydrogen, a set of Feynman diagrams can be generated, which can be associated with energy shifts with the use of either S-matrix techniques, used in Ref. [15], or two-time Green's function techniques [18], used in Ref. [16]. The diagrams are similar to those used in hydrogen calculations, although, as we shall show later, new diagrams involving photon exchange between different electrons and a new interaction associated with the model potential $U(r)$ are present.

As individual contributions to the energy level change with $U(r)$, only if E_D can be shown to be independent of the potential to a high degree of accuracy will this approach be of practical utility. This is definitely not the case for most neutral atoms, although Hamiltonian methods that sum high orders of MBPT diagrams such as coupled-cluster methods [19] are constantly improving. However, it is the case for the isoelectronic sequences mentioned above once the ions are highly charged. In this case one need consider only a limited set of Feynman diagrams, and a well-defined way of carrying out completely QED-based calculations of the ions exists. As will be described below, QED effects get intertwined to some extent with the definition of E_D, so in the following we give results solely in terms of Feynman diagrams.

The extension from lithiumlike to the general case is complicated by a number of issues. The first has to do with the starting point of the calculations, which can be chosen to be hydrogenic orbitals for lithiumlike ions. However, with 11 or more electrons, ignoring the electron-electron interaction in lowest order is a poor approximation. This necessitates building in screening in the basic formalism, an optional step for the lithium isoelectronic sequence. Second, the fact that only the $1s$ core state was populated in lithiumlike ions led to certain simplifications, so some of the formulas given in Ref. [15] have to be generalized to the case when there are multiple core states. Third, an interesting apparent instability appears in two parts of the two-photon exchange calculation. The combination of those parts will be shown to be stable, and the reason for the instability, which is related to autoionizing states, is discussed. Finally, even though the large nuclear mass makes recoil corrections small, the QED treatment is highly nontrivial, and will be discussed in some detail.

The plan of the paper is as follows. In the next section, we introduce the formalism used in the calculations. In the following three sections we treat energy shifts associated with Feynman diagrams with one, two, and three photons, respectively. The finite mass of the nucleus is accounted for, along with a discussion of issues to do with its structure in Sec. VI. Application to the sodium isoelectronic sequence is given in Sec. VII, along with a comparison with other calculations and experiment. In the conclusion we discuss issues involved in carrying out a more complete QED treatment of alkali-metal-like ions, and the possibility of treating ions with more complicated electronic structure.

II. *S*-MATRIX FORMALISM

The fact that even the lightest nucleus is three orders of magnitude heavier than the electron leads to its role being predominantly the source of a classical Coulomb field. Once this approximation is made, one is dealing with a standard bound-state QED problem that can be treated in the Furry representation [2]. While the original application was to hydrogen, QED is intrinsically a many-body theory, and one can treat atoms with more than one electron with the same formalism. In terms of creation and annihilation operators, all that needs to be done for alkali-metal-like ions is to change the initial state of an electron in state v, for hydrogen described as

$$|v\rangle = b_v^\dagger\,|0\rangle, \tag{7}$$

to

$$|v\rangle = b_v^\dagger\,|0_C\rangle. \tag{8}$$

Here $|0\rangle$ is a state with no electrons present, and $|0_C\rangle$ a state with all core states populated, ten for the case of sodiumlike ions.

While QED is intrinsically a many-body theory, the electron propagator does not automatically "know" how many electrons are present when one is doing calculations on a many-electron atom or ion. This leads to certain complications when carrying out practical calculations. Many of these are avoided in MBPT through a redefinition of the ground state. While similar redefinitions can be done in QED, here we choose the ground state to have no core electrons present. This means that for sodiumlike ions $|0_C\rangle$ is understood to have ten core electron creation operators operating on $|0\rangle$. We will show in several cases throughout the paper how different Feynman diagrams act together to effectively "fill the core," building in the effect of the Pauli exclusion principle by canceling terms involving core electrons.

We begin by showing in the row labeled $E0$ in Tables I and II the $3s$, $3p_{1/2}$, and $3p_{3/2}$ eigenenergies of sodiumlike

TABLE I. Breakdown of structure and QED contributions to the ionization potentials (a.u.) of the $n = 3$ states for sodiumlike tungsten using the Coulomb potential.

Terms	$3s_{1/2}$	$3p_{1/2}$	$3p_{3/2}$
$E0$	−330.1011	−330.1498	−311.9187
$E1$	71.2399	78.3267	73.4074
$E2$	−3.4203	−4.4226	−4.0129
$E3$	0.0091	0.0104	0.0028
Recoil 1	0.0011	0.0010	0.0009
Recoil 2	−0.0001	−0.0005	−0.0005
SE	0.2856	0.0267	0.0394
Uehling	−0.0515	−0.0061	−0.0005
WK	0.0019	0.0003	0.0001
SE screen	−0.0659	−0.0186	−0.0291
VP screen	0.0118	0.0038	0.0015
Sum	−262.0895	−256.2335	−242.5096

tungsten in two different potentials. Sodiumlike tungsten is the ion we use for purposes of illustration. It is also of current interest, as recent experiments [20,21] have found

$$E_{3p_{1/2}} - E_{3s_{1/2}} = 5.8635(12)\text{a.u.},$$
$$E_{3p_{3/2}} - E_{3s_{1/2}} = 19.595(5)\text{a.u.}$$

We note that natural units with $\hbar = c = 1$ are used throughout this paper, and unless otherwise specified, energies are given in atomic units, where 1 a.u. $= 27.211\,384$ eV.

Were we to start by ignoring the interaction between electrons, we would be using the original Furry representation, which has the external field being the Coulomb field of the nucleus,

$$U_C(r) = -\frac{\alpha Z_{\rm nuc}(r)}{r}. \tag{9}$$

Solving the Dirac equation for a nucleus of finite size with root-mean-square charge radius of 5.359 fm gives the Coulomb eigenenergies $E0$ shown in Table I, which leads to transition energies of −0.048 and 18.182 a.u., a clearly undesirable starting point. However, the Furry representation can easily be modified by taking the QED Hamiltonian $H = H_0 + H_I$ and rearranging it to $H = \tilde{H}_0 + \tilde{H}_I$, where

$$\tilde{H}_0 = \int d^3x\, \psi^\dagger(x)[-i\vec{\alpha}\cdot\vec{\nabla} + \beta m + U_C(r) + U(r)]\psi(x), \tag{10}$$

with $U(r)$ chosen to approximately account for the effect of screening. This requires a modification of the interaction Hamiltonian, which acquires a new counterterm,

$$H_{\rm CT} = -\int d^3x\, \psi^\dagger(x)U(r)\psi(x), \tag{11}$$

so that the interaction Hamiltonian becomes

$$\tilde{H}_I = \int d^3x[q_e A^\mu(x)\bar{\psi}(x)\gamma_\mu\psi(x) - \psi^\dagger(x)U(r)\psi(x)]. \tag{12}$$

We use Feynman gauge for this part of the calculation, but note that we will later use Coulomb gauge when recoil corrections are treated. In the above equations $\psi(x)$ is a field operator, with associated wave functions obeying the Dirac equation

$$[-i\vec{\alpha}\cdot\vec{\nabla} + \beta m + U_C(r) + U(r)]\psi_n(\vec{x}) = \epsilon_n\psi_n(\vec{x}). \tag{13}$$

We can choose any function $U(r)$, so long as it is a local function of r, which prohibits use of the Hartree-Fock potential. However, a local potential that gives results close to those of the Hartree-Fock potential is the Kohn-Sham (KS) potential [22], which we define as $V_{\rm KS}(r) = U_C(r) + U_{\rm KS}(r)$, with

$$U_{\rm KS}(r) = \alpha\int dr'\,\frac{1}{r_>}\,\rho_t(r') - \frac{2}{3}\left[\frac{81}{32\pi^2}\,r\rho_t(r)\right]^{1/3}\frac{\alpha}{r}. \tag{14}$$

Here

$$\rho_t(r) = g_v^2(r) + f_v^2(r) + \sum_a (2j_a+1)\left[g_a^2(r) + f_a^2(r)\right], \tag{15}$$

where the large- and small-component radial Dirac wave functions g and f are normalized so that, for large r, $U_{\rm KS}(r) \to \alpha N/r$, with N the number of electrons. For the sodium isoelectronic sequence, the valence state v is chosen to be the $3s$ state, and the sum over the core states a ranges over the $1s$, $2s$, $2p_{1/2}$, and $2p_{3/2}$ states. Solving the Dirac equation with this potential gives the results $E0$ on the first line of Table II, and we now have a starting point within 6% for the $3s_{1/2}$-$3p_{1/2}$ transition energy and (accidentally) almost exactly in agreement with the $3s_{1/2}$-$3p_{3/2}$ transition energies. In our earlier calculation on lithiumlike bismuth [23], we chose a set of potentials, which of course gave different transition energies in lowest order, and showed that inclusion of higher-order diagrams led to well-converged totals: here we will do this only for the case of sodiumlike tungsten.

We now wish to begin including the corrections coming from $\tilde{H}_I$. This can be done by using the S matrix, the time-ordered exponential of the sum of these interaction Hamiltonians. Carrying out the standard expansion of the S matrix leads to expressions that can be represented by Feynman diagrams. To deal with bound-state QED the rules for these diagrams must be slightly modified, as we wish to calculate energies rather than scattering amplitudes. To do this, an adiabatic damping factor $e^{-\varepsilon|t|}$ is introduced that multiplies the interaction Hamiltonian, and one can then show that energy

TABLE II. Breakdown of structure and QED contributions to the ionization potentials (a.u.) of the $n = 3$ states for sodiumlike tungsten using the Kohn-Sham potential.

Terms	$3s_{1/2}$	$3p_{1/2}$	$3p_{3/2}$
$E0$	−260.1538	−254.6228	−240.5712
$E1$	−2.0688	−1.5423	−1.8936
$E2$	−0.0460	−0.0638	−0.0517
$E3$	0.0004	0.0006	0.0005
Recoil 1	0.0009	0.0008	0.0008
Recoil 2	−0.0001	−0.0004	−0.0004
SE	0.2326	0.0186	0.0291
Uehling	−0.0421	−0.0044	−0.0003
WK	0.0015	0.0002	0.0000
SE screen	−0.0109	−0.0096	−0.0078
VP screen	0.0018	0.0017	0.0012
Sum	−262.0845	−256.2214	−242.4934

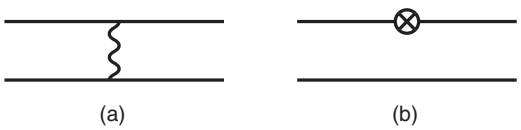

FIG. 1. (a) One-photon exchange diagram between the valence and a core electron and (b) the action of a counterpotential, represented by a cross inside a circle, on a valence electron.

shifts can be obtained from this modified Hamiltonian with the equation [24]

$$\Delta E = \lim_{\varepsilon\to 0}\frac{i\varepsilon}{2}\lim_{\lambda\to 1}\frac{\frac{\partial}{\partial\lambda}\langle\phi|T(e^{-i\lambda\bar{H}_I})|\phi\rangle}{\langle\phi|T(e^{-i\lambda\bar{H}_I})|\phi\rangle}, \tag{16}$$

where

$$\bar{H}_I \equiv \int dx_0\, e^{-\varepsilon|x_0|}\tilde{H}_I. \tag{17}$$

Note that the first term in the perturbation expansion of $\langle\phi|T(e^{-i\lambda\bar{H}_I})|\phi\rangle$ is 1, so the denominator in the above can often be neglected, but it will play a role in the evaluation of two-photon terms.

At this point corrections can be calculated using the standard tools of quantum field theory. A frequently encountered integral when Feynman gauge is used is

$$g_{ijkl}(E) = \alpha\int d^3x\, d^3y\,\frac{e^{i\bar{E}R}}{R}\,\psi_i^\dagger(\vec{x})\alpha_\mu\psi_k(\vec{x})\,\psi_j^\dagger(\vec{y})\alpha^\mu\psi_l(\vec{y}), \tag{18}$$

where $R = |\vec{x}-\vec{y}|$, $\alpha^\mu = (1,\vec{\alpha})$, and $\bar{E} = \sqrt{E^2 + i\delta}$. If we restrict μ to 0 and put $E = 0$ this is the familiar Coulomb matrix element of MBPT, g^c_{ijkl}. The definition of $\bar{E}$ builds in the proper boundary conditions: for real values of E it is of course simply the absolute value, and when we need to deal with complex values it gives exponential damping.

III. ONE-PHOTON EFFECTS

A. One-photon exchange terms

In Fig. 1, we show the diagrams for the exchange of a photon between the valence electron and a core electron, together with the action of $H_{\rm CT}$ on a valence electron: in terms of counting photons, one $H_{\rm CT}$ always counts as 1, but one needs two actions of $A^\mu\bar{\psi}\gamma_\mu\psi$ to get a photon propagator. Diagrams in which the valence electron is not involved, while they do not vanish, can be ignored for our purposes, as they affect neither valence removal or transition energies, and the convention of not including diagrams of this sort will be followed throughout the calculation. The photon propagator in Feynman gauge is

$$\begin{aligned} D_{\mu\nu}(x,y) &= -g_{\mu\nu}\int\frac{d^4k}{(2\pi)^4}\,\frac{e^{-ik\cdot(x-y)}}{k^2+i\delta} \\ &= g_{\mu\nu}\,\frac{1}{4\pi R}\int\frac{dk_0}{2\pi}\,e^{i|k_0|R}, \end{aligned} \tag{19}$$

where $R = |\vec{x}-\vec{y}|$, and we use a metric where $k^2 = k_0^2 - \vec{k}^2$. The integral over x_0 gives a function multiplying this of the form

$$D_\varepsilon = \frac{\varepsilon}{\pi}\,\frac{1}{\varepsilon^2 + (k_0 - E)^2}, \tag{20}$$

where for this problem $E = 0$ or $E = \epsilon_v - \epsilon_a$. This acts as a δ function, and one can usually set $k_0 = E$ in Eq. (20). Evaluating the integral over k_0 then gives a term varying as $1/\varepsilon$, which cancels the ε in Eq. (16). After carrying out the simpler analysis of the counterterm graph, one finds the energy shift

$$E_{1F} = \sum_a\left[g_{vava}(0) - g_{vaav}(\epsilon_{va})\right] - U_{vv}, \tag{21}$$

where we have introduced the notation

$$\epsilon_{ij} \equiv \epsilon_i - \epsilon_j. \tag{22}$$

If we replace g with g^c this exactly reproduces the energy that would be found in MBPT. We are using Feynman gauge, but note that if we used Coulomb gauge, the replacement just mentioned is exactly the result of calculating the exchange of a Coulomb photon. In Coulomb gauge one also has transverse photons, but their connection to Feynman gauge is more complicated. However, because we are working with a local potential, gauge invariance ensures that the results of a Feynman gauge calculation will be identical to those coming from a Coulomb gauge calculation so long as a gauge-invariant set of diagrams is treated.

The term involving g_{vaav} has in general both a real and an imaginary part, with the latter playing a role in the decay rate of the ion, discussed further below. We do not tabulate it here, as we are interested in energies, but note that the imaginary parts of g terms have to be kept when more than one of them are present, as is the case for two-photon contributions. The real part is given as $E1$ in Tables I and II. We note that if we compare the $3s$ energy for the two potentials, a 0.2% discrepancy in lowest order is reduced to 0.03% after $E1$ is included.

FIG. 2. One-photon self-energy and vacuum polarization diagrams for the valence electron.

B. One-loop Lamb shift diagrams

Turning to the other one-photon diagrams, the self-energy (SE) and vacuum polarization (VP) shown in Fig. 2, we note that the techniques we use for their evaluation have been described in considerable detail in Refs. [25,26]. The calculations apply to any state, so we do not repeat the formulas here. However, there are corrections to the SE term not important in lowest order that need to be discussed for later application in the two-photon calculation. If we define the electron self-energy operator as

$$\begin{aligned} \Sigma_{ij}(\epsilon) = -ie^2\int d^3x\, d^3y\int\frac{d^nk}{(2\pi)^n}\,\frac{e^{i\vec{k}\cdot(\vec{x}-\vec{y})}}{k^2+i\delta}\,\bar{\psi}_i(\vec{x})\gamma_\mu \\ \times S_F(\vec{x},\vec{y};\epsilon - k_0)\gamma^\mu\psi_j(\vec{y}), \end{aligned} \tag{23}$$

the self-energy contribution for the valence election is $\Sigma_{vv}(\epsilon_v)$. (A self-mass counterterm is implicit.) The electron propagator S_F, which satisfies

$$\{[E - U_C(r) - U(r)]\gamma_0 + i\vec{\gamma}\cdot\vec{\nabla}_x - m\}S_F(\vec{x},\vec{y};E) = \delta^3(\vec{x}-\vec{y}), \tag{24}$$

is treated in two ways throughout this calculation. The first utilizes a spectral decomposition, represented by a sum over positive and negative energy states,

$$S_F(\vec{x},\vec{y};E) = \sum_m \frac{\psi_m(\vec{x})\bar{\psi}_m(\vec{y})}{E - \epsilon_m(1 - i\delta)}. \tag{25}$$

The term involving δ puts poles in the complex E plane below the positive real axis for positive energy states and above the negative real axis for negative energy states. This form for the propagator is very useful, and fits in with one of our numerical methods, the use of finite basis sets [27]. These methods allow us to replace the sum in the spectral decomposition, which has an infinite sum over bound states along with an integration over continuum states, with a finite sum, for a typical basis set of a given angular momentum channel involving 50 negative energy states and 50 positive energy states. The number 50 is chosen because calculations of terms involving S_F have generally converged by that point, with the use of larger basis sets not changing the answer appreciably.

The other method of treating the electron propagator uses differential equation techniques. There, one solves the Dirac equation away from an energy eigenvalue. Two types of solution result, one which is finite at the origin but diverges at infinity, and the other with the situation reversed. $S_F(\vec{x},\vec{y};E)$ can then be formed as a linear combination of products of these functions. This method is particularly useful when high accuracy is called for.

The SE term is ultraviolet divergent, and we have regularized that divergence by replacing d^4k with d^nk where $n = 4 - 2\epsilon_d$, with the understanding that $\epsilon_d \to 0$ after renormalization. Were we to take ϵ_d to vanish, the SE term would be, after carrying out the d^3k integration and using Eq. (18),

$$\Sigma_{vv}(\epsilon_v) = -i\int \frac{dk_0}{2\pi}\sum_m \frac{g_{vmmv}(k_0)}{k_0 - \epsilon_v + \epsilon_m(1 - i\delta)}. \tag{26}$$

To numerically evaluate this, we Wick-rotate k_0 to the imaginary axis, $k_0 \to i\omega$. The integration over ω is divergent, and a subtraction scheme is required to make it finite, but here we concentrate on the effect of states more deeply bound than the valence state on the Wick rotation. These lead to poles that are encircled by this rotation, which give a contribution to the self-energy we refer to as the pole term,

$$\Sigma_{vv}[p] = \sum_p g_{vppv}(\epsilon_{vp}), \tag{27}$$

where p sums over all more deeply bound states. The special case $p = v$ will be discussed below. We note the similarity of the pole term to the second term in E_{1F}, differing only by having the opposite sign and summing over both the core and any valence states with less energy than ϵ_v. These terms generally have real and imaginary parts. They are the only source of an imaginary part to the energy from one-loop radiative corrections, as the ω integration is purely real, as are the vacuum polarization corrections.

The fact that the pole term is almost the negative of the second term of E_{1F} shows a connection between topologically different diagrams that will be encountered again when we discuss two-photon physics. This cancellation of the core terms is needed to enforce the Pauli exclusion principle in our approach, since the valence electron in an alkali-metal-like ion cannot decay to a core state a. Were we dealing with a hydrogenic ion and v was any state above the $1s$ state, no one-photon diagram would exist to lead to a cancellation, and decays to all lower-energy states, unless prohibited by parity or angular momentum considerations, would be possible.

At this point we elaborate on the pole term when $p = v$. This is actually a half pole, and a factor of $1/2$ should be present for that case since that pole is not encircled by the Wick rotation, but only skirted with a half circle. However, in order to deal with singularities in parts of the two-photon calculation we have introduced what we call "reference-state regularization." It is distinct from the usual infrared and ultraviolet regularizations encountered in QED. It consists of introducing a small parameter δ and the replacement of the actual valence and core energies (in this case including the rest mass of the electron) with

$$\begin{aligned}\epsilon_v &\to \epsilon_v(1-\delta),\\ \epsilon_a &\to \epsilon_a(1 - \delta\,\epsilon_v/\epsilon_a).\end{aligned} \tag{28}$$

This regulates certain terms, discussed in more detail in Sec. IV, that would diverge logarithmically to become factors of $\ln\delta$. We generally take the average of a small positive and a small negative δ, and this procedure leads to the factor $1/2$ in the pole term when $p = v$.

IV. TWO-PHOTON PHYSICS

A. Two-photon exchange terms

Before beginning the S-matrix calculation, we note that second-order MBPT gives an important contribution to energies of highly charged ions, as it behaves as Z^0 in the $1/Z$ expansion. We wish to show that it can be obtained as a limit of the diagrams in which two photons are exchanged between electrons. The MBPT formula is

$$\begin{aligned}E^{(2)} = &\sum_{abm}\frac{g^c_{mvba}\left(g^c_{abmv} - g^c_{abvm}\right)}{\epsilon_a + \epsilon_b - \epsilon_m - \epsilon_v}\\ &+ \sum_{amn}\frac{g^c_{avmn}\left(g^c_{mnav} - g^c_{mnva}\right)}{\epsilon_a + \epsilon_v - \epsilon_m - \epsilon_n}\\ &+ \sum_{am}\frac{X_{am}\left(g^c_{vmva} - g^c_{viav}\right) + \left(g^c_{vavm} - g^c_{vamv}\right)X_{ma}}{\epsilon_a - \epsilon_m}\\ &+ \sum_i \frac{X_{vi}X_{iv}}{\epsilon_v - \epsilon_i}.\end{aligned} \tag{29}$$

Here $X \equiv V_{\rm HF} - U$, where

$$(V_{\rm HF})_{ij} = \sum_a \left(g^c_{iaja} - g^c_{iaaj}\right). \tag{30}$$

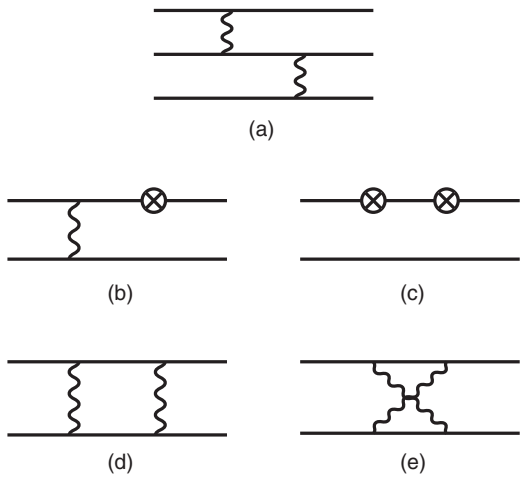

FIG. 3. Two-photon exchange diagrams between the valence and up to two core electrons. A cross inside a circle represents a counterpotential. Where there is no photon exchanged between electrons (c), core electrons are treated as spectators only.

We follow the usual MBPT notation that $a, b, \ldots$ sum over only occupied core states, $m, n, \ldots$ sum over positive energy states above the core, and $i, j, \ldots$ sum over both. For purposes of comparison with the part of the S-matrix calculation related to this contribution, we note that we can rewrite $E^{(2)}$ in terms of a unrestricted summation over i and j by simply carrying out manipulations like

$$\sum_m F(m) = \sum_i F(i) - \sum_a F(a). \tag{31}$$

The result of this exercise casts Eq. (29) into the form

$$\begin{aligned} E^{(2)} = &\sum_{abi} \frac{g^c_{ivba}\left(g^c_{abiv} - g^c_{abvi}\right)}{\epsilon_a + \epsilon_b - \epsilon_i - \epsilon_v} + \sum_{aij} \frac{g^c_{avij}\left(g^c_{ijav} - g^c_{ijva}\right)}{\epsilon_a + \epsilon_v - \epsilon_i - \epsilon_j} \\ &- \sum_{abi} \frac{\left(g^c_{avib} - g^c_{avbi}\right)\left(g^c_{ibav} - g^c_{ibva}\right)}{\epsilon_a + \epsilon_v - \epsilon_i - \epsilon_b} \\ &+ \sum_{ai} \frac{X_{ai}\left(g^c_{viva} - g^c_{viav}\right) + \left(g^c_{vavi} - g^c_{vaiv}\right)X_{ia}}{\epsilon_a - \epsilon_i} \\ &+ \sum_i \frac{X_{vi}X_{iv}}{\epsilon_v - \epsilon_i}. \end{aligned} \tag{32}$$

In this form the relation between MBPT and the present S-matrix calculation is clearest.

Now turning to the present two-photon exchange calculation, we note that it leads to a number of effects, which we organize by the number of closed loops. The simplest diagrams have no loops, and we begin with them. They are shown in Figs. 3(a)–3(c). The two-photon propagators can be treated as described above, with the lowest-order approximation giving

$$\begin{aligned} E_{2F} = &\sum_{abi} \frac{[g_{bvbi}(0) - g_{vbbi}(\epsilon_{vb})]\,[g_{iava}(0) - g_{iaav}(\epsilon_{va})]}{\epsilon_v - \epsilon_i} + \sum_{abi} \frac{[g_{vavi}(0) - g_{vaiv}(\epsilon_{av})]\,[g_{ibab}(0) - g_{ibba}(\epsilon_{ab})]}{\epsilon_a - \epsilon_i} \\ &+ \sum_{abi} \frac{[g_{viva}(0) - g_{ivva}(\epsilon_{av})]\,[g_{abib}(0) - g_{abbi}(\epsilon_{ab})]}{\epsilon_a - \epsilon_i} - \sum_{abi} \frac{[g_{avbi}(\epsilon_{ab}) - g_{avib}(\epsilon_{vb})]\,[g_{ibva}(\epsilon_{ab}) - g_{ibav}(\epsilon_{vb})]}{\epsilon_a + \epsilon_v - \epsilon_i - \epsilon_b} \\ &+ \sum_{abi} \frac{[g_{bavi}(\epsilon_{vb}) - g_{abvi}(\epsilon_{va})]g_{ivba}(\epsilon_{va})}{\epsilon_a + \epsilon_b - \epsilon_v - \epsilon_i} - \sum_{ai} \frac{[g_{avai}(0) - g_{vaai}(\epsilon_{va})]\,U_{iv} + U_{vi}\,[g_{aiav}(0) - g_{iaav}(\epsilon_{va})]}{\epsilon_v - \epsilon_i} \\ &- \sum_{ai} \frac{[g_{aviv}(0) - g_{vaiv}(\epsilon_{va})]\,U_{ia} + U_{ai}\,[g_{ivav}(0) - g_{ivva}(\epsilon_{va})]}{\epsilon_a - \epsilon_i} + \sum_i \frac{U_{vi}\,U_{iv}}{\epsilon_v - \epsilon_i}. \end{aligned} \tag{33}$$

We first note that the first, sixth, and eighth terms, if we replace $g(E)$ with g^c, reproduce the last term of Eq. (32). Similarly, the second, third, and seventh terms reproduce the next to last term. The fourth term reproduces the third term, and the fifth the first term. Only the second term of Eq. (32) remains unaccounted for, and we will see below that it can be found in a one-loop diagram.

In the above expressions, terms in which the denominator vanishes are understood to be excluded. While this is automatic in MBPT, the treatment of these terms requires care in the present approach. The excluded terms lead to contributions with an extra power of $1/\epsilon$. The leading part of the contribution cancels with a term arising from expanding the denominator of Eq. (16), but when matrix elements $g_{ijkl}(E)$ are taken together with the function D_ϵ of Eq. (20), an extra term arises from Taylor-expanding $g_{ijkl}(E) = g_{ijkl}(k_0) + (E - k_0)g'_{ijkl}(k_0)$. A detailed description of how this works can be found in Sec. II B of Ref. [28]. These terms are the first of a set of contributions to the energy that we call derivative terms, which all arise from similar manipulations. In this case they are

$$\begin{aligned} E_{2F'} = &\sum_{ab} g'_{avvb}(\epsilon_{va})[g_{vbva}(0) - g_{vbav}(\epsilon_{va})] \\ &- \sum_{ab} g'_{vbav}(-\epsilon_{va})[g_{vaba}(0) - g_{vaab}(0)] \\ &- \sum_{ab} g'_{vbbv}(\epsilon_{va})[g_{vava}(0) - g_{vaav}(\epsilon_{va})] \\ &+ U_{vv} \sum_a g'_{vaav}(\epsilon_{va}) + \sum_a U_{[a][a]}g'_{vaav}(-\epsilon_{va}). \end{aligned} \tag{34}$$

We note that particular care must be taken in this derivation, because while $g(E)$ is an even function, $g'(E)$ is odd, so the signs of the arguments in the above are important. The matrix

element of U does not depend on the magnetic quantum number of core state a, which we emphasize with the $[a]$ notation.

Evaluation of these terms is computationally simple. However, the numerical evaluation of one of them is unstable. This instability comes from the fourth term in E_{2F}. If we write the negative of the denominator as $\epsilon_i - (\epsilon_v + \Delta)$, with $\Delta = \epsilon_a - \epsilon_b$, we first note that for lithiumlike ions, Δ vanishes as there is only one $1s$ core state, and the denominator vanishes only for the case that is eliminated by the formalism. However, for ions with more than one core state, Δ can be large and sufficiently positive so as to make the sum $\epsilon_v + \Delta$ an energy in the continuum. This should always lead to a vanishing denominator, characteristic of autoionizing states. We note that such terms are not present in Eq. (29), the equation for MBPT. However, they do appear in Eq. (32), which resulted from the manipulation in which we forced intermediate sums to include the core. This suggests that the instability is spurious, and we will show below that this is indeed the case.

This numerical problem could be severe if, for example, we attempted to use differential equation techniques, which implicitly include core states, to carry out the sum over i. However, we chose to evaluate this term with finite-basis-set techniques [27], in which ϵ_i ranges over a set of discrete values. While it is extremely unlikely that one value would precisely lead to a vanishing energy denominator, these discrete values change as the basis set changes, and this affects the answer. The instability referred to above is the fact that as the basis set is increased in size, E_{2F}, rather than tending to a converged value as is usually the case with finite-basis-set calculations, keeps changing its value regardless of how large the basis set is made due to the changing value of $\epsilon_v + \Delta$. However, as with the one-photon case, the terms causing the problem can be shown to cancel with part of the other two-photon exchange diagram involving one loop. Before discussing that, we again emphasize that the two g factors in each term are both complex numbers, and the calculation is carried out with that in mind. However, while the end result has an imaginary part, we do not evaluate it here, and will keep only the real part of all further two-photon terms. Presumably, were one to follow all imaginary terms from two-photon physics, one would again find canceling terms enforcing the Pauli exclusion principle, along with reproducing the two-photon decay rate and radiative corrections to one-photon decay.

B. Ladder and crossed-ladder diagrams

We now turn to the one-loop diagrams, which can be broken into two classes, one primarily associated with structure and the other with screening of the Lamb shift. The structure diagrams are shown in Figs. 3(d) and 3(e), which we refer to as the ladder (L) and crossed-ladder (X) diagrams, respectively. They give the energy shifts

$$\Delta E_L = \frac{i}{2\pi}\sum_{aij}\int_{-\infty}^{\infty} dz \times \frac{g_{ijav}(z)[g_{avij}(z) - g_{avji}(z-\epsilon_{va})]}{[\epsilon_a + z - \epsilon_i(1-i\delta)]\,[\epsilon_v - z - \epsilon_j(1-i\delta)]} \quad (35)$$

and

$$\Delta E_X = \frac{i}{2\pi}\sum_{aij}\int_{-\infty}^{\infty} dz \times \left\{\frac{g_{ajiv}(z)g_{ivaj}(z)}{[\epsilon_a + z - \epsilon_i(1-i\delta)]\,[\epsilon_v + z - \epsilon_j(1-i\delta)]} - \frac{g_{ajia}(z)g_{ivvj}(z-\epsilon_{va})}{[\epsilon_a + z - \epsilon_i(1-i\delta)]\,[\epsilon_a + z - \epsilon_j(1-i\delta)]}\right\}. \quad (36)$$

At this point we can complete the connection to MBPT. If we again replace $g(E)$ with g^c, Cauchy's theorem allows the z integration to be carried out. For the ladder, if both intermediate states are positive energy states, the second term of Eq. (32) is reproduced, which was the only term from Eq. (32) that had not already been accounted for.

There is of course additional physics present even with the approximation we have made. For the ladder, while terms with one positive and one negative energy state vanish, a contribution survives when both are negative. For the crossed ladder, the nonvanishing terms after Cauchy integration involve one positive and one negative energy state. Power-counting arguments can be made that show these three extra contributions contribute at the level of $1/Z$ of the one-loop Lamb shift, that is, $(Z\alpha)^3$ a.u., and they can be thought of as being part of the screening of the Lamb shift. We will return to the connection of MBPT and QED in the three-photon section, but now continue with the numerical evaluation of the ladder and crossed-ladder diagrams.

While the basic formulas for ΔE_L and ΔE_X are relatively simple, and the z integration easily evaluated in the MBPT approximation, the unapproximated integrals are quite complicated to carry out. The main problem has to do with the fact that, just as with the one-loop self-energy, a Wick rotation $z \to i\omega$ is called for. However, the structure of the complex plane now has not only a set of poles that get encircled, sometimes appearing as double poles, but also has two cuts that must be wrapped around. We begin by treating the pole terms.

For the ladder, if we choose to close the contour from above, we need to consider poles in quadrants I and III. The first part of the denominator has poles when

$$z = -\epsilon_a + \epsilon_i(1 - i\delta). \quad (37)$$

We will rename i as p_1 if it is encircled. For negative ϵ_i the poles are in quadrant II, and for positive ϵ either III or IV. To be in quadrant III requires $\epsilon_{p1} \leqslant \epsilon_a$, that is, p_1 is a core state more deeply bound than whichever core state a is under consideration. Summing over all such states gives

$$\Delta E_L(p_1) = \sum_{ap_1i}\left[\frac{g_{p_1iav}(\epsilon_{p_1a})g_{avp_1j}(\epsilon_{p_1v})}{\epsilon_a + \epsilon_v - \epsilon_{p_1} - \epsilon_i} - \frac{g_{p_1iav}(\epsilon_{p_1a})g_{avip_1}(\epsilon_{p_1a})}{\epsilon_a + \epsilon_v - \epsilon_{p_1} - \epsilon_i}\right]. \quad (38)$$

The second part of the denominator has poles when

$$z = \epsilon_v - \epsilon_j(1 - i\delta). \quad (39)$$

In this case negative energy states have poles in quadrant IV, and positive energy states have poles in quadrant I, but only

when $\epsilon_v \geqslant \epsilon_{p_2}$. This gives rise to

$$\Delta E_L(p_2) = \sum_{ap_2i} \left[\frac{g_{ip2av}(\epsilon_{vp_2}) g_{avip2}(\epsilon_{vp_2})}{\epsilon_a + \epsilon_v - \epsilon_{p_2} - \epsilon_i} - \frac{g_{ip2av}(\epsilon_{vp_2}) g_{avp_2i}(\epsilon_{ap_2})}{\epsilon_a + \epsilon_v - \epsilon_{p_1} - \epsilon_i} \right]. \quad (40)$$

When these ladder pole terms are evaluated numerically with finite-basis-set techniques, the same instability as encountered in E_{2F} appears. However, the terms that give rise to the instability can be seen to be equal and opposite in the two cases, so the sum is stable. We note that the cancellation is only of the unstable terms because the p_1 poles do not range over the entire core. Furthermore, we do not explicitly build in the cancellation, instead evaluating E_{2F} and the sum of all pole terms from the ladder and crossed-ladder diagrams separately. While each has the instability, the sum is completely stable.

The analysis of the crossed-ladder poles is done in a manner similar to that of the ladder poles. The rest of the calculation follows exactly along the lines given for the treatment of excited states of helium given in [28]. As with our work on lithiumlike ions [15], the ω integration that remains after the poles and cuts have been dealt with is by far the most computationally intensive part of the calculation. We carried this out with both finite-basis-set and differential equation techniques, as described in that paper. The sum of the two-photon structure diagrams is denoted $E2$ in Tables I and II. It is notable that this rather involved set of calculations gives a result quite close to that of the MBPT procedure of Ref. [11], even though MBPT excludes contributions from the negative energy states and its treatment of retardation is less complete than the present approach.

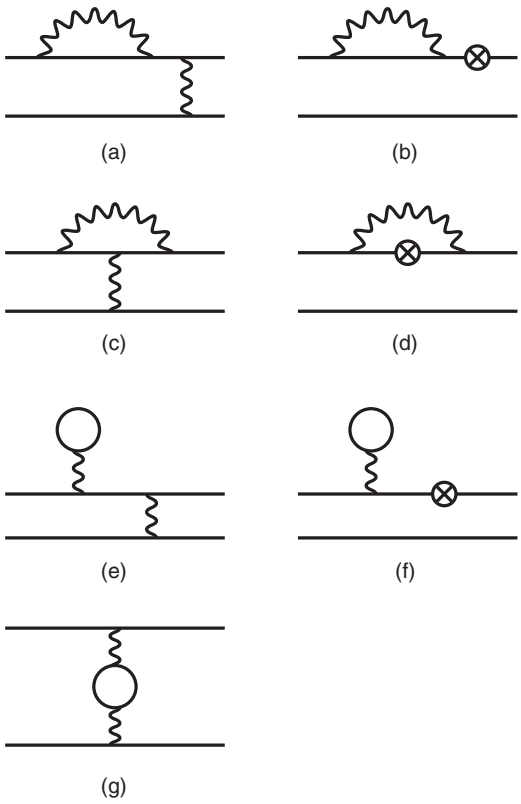

FIG. 4. Screened self-energy (a)–(d) and vacuum polarization (e)–(g) diagrams between the valence and a core electron. A cross inside a circle represents a counterpotential. Where there is no photon exchanged between electrons (b),(d),(f), core electrons are treated as spectators only.

C. Lamb shift screening diagrams

The one-loop self-energy has had some screening built into it by our choosing a screened potential. For example, from Table I, with only the nuclear Coulomb field present, the $3s$ self-energy is 0.2856 a.u. and the Uehling potential -0.0515 a.u. Referring to Table II, we see that the screening provided by the KS potential is 18% for both. The diagrams of Fig. 4 provide further screening (or antiscreening, if the original potential provides too much screening).

The treatment of these diagrams is almost completely unchanged from that described in Ref. [15] for lithiumlike ions because, regardless of the number of core electrons present, only one photon is exchanged, with the other being part of the radiative correction. Therefore the valence state can interact with only one core state at a time. Thus, for the most part, for alkali-metal-like ions one simply carries out a calculation for each core state similar to that described in Ref. [15] and sums them. There is always a sum over the magnetic quantum number of the core state, and when one does not have an s state there is a more complicated angular momentum recoupling factor associated with summing over all magnetic quantum numbers; otherwise the calculation is basically unchanged. For example, the derivative term coming from the valence line,

$$E_v(\text{der}) = E_{1F}\, \Sigma'_{vv}(\epsilon_v) - \sum_a g'_{vaav}(\epsilon_{va})\, \Sigma_{vv}(\epsilon_v), \quad (41)$$

is unchanged from Eq. (22) of Ref. [23], but for derivatives coming from the core states, Eq. (23) of that work must be changed to

$$E_{\text{core}}(\text{der}) = \sum_a \Sigma'_{[a][a]}(\epsilon_a)[g_{vava}(0) - g_{vaav}(\epsilon_{av})] - \sum_a \Sigma_{[a][a]}(\epsilon_a) g'_{avva}(\epsilon_{av}). \quad (42)$$

The same issues as discussed after Eq. (34) enter here, namely, care is needed with the sign of the argument of g' and the notation $[a]$ is used to emphasize magnetic quantum number independence.

The derivative term comes from the part of the spectral representation of the electron propagator in Figs. 4(c) and 4(d) when $\epsilon_m = \epsilon_v$, to be discussed in connection to the vertex diagrams below. When $\epsilon_m \neq \epsilon_v$ the sum over m generates what we call a "perturbed orbital" term. Such terms were treated in a general way in Ref. [23], where they were denoted as $\tilde{v}$ or $\tilde{a}$. Because the self-energy is diagonal in magnetic quantum numbers one can eliminate them from the sum over the core

and write

$$\Delta E_{\rm PO} = \Sigma_{v\tilde{v}}(\epsilon_v) + \Sigma_{\tilde{v}v}(\epsilon_v) + \sum_{[a]}(2j_a+1)\big[\Sigma_{[a][\tilde{a}]}(\epsilon_a) + \Sigma_{[\tilde{a}][a]}(\epsilon_a)\big]. \quad (43)$$

In the lithiumlike work [15], a simple factor of 2 was used.

The vertex diagrams of Figs. 4(c) and 4(d) were also treated in generality in Ref. [15], with the state a left unspecified. As shown in [15], they consist of five terms: ΔE_1 – ΔE_5 where ΔE_1 and ΔE_2 are the direct and exchange terms of Fig. 4(c) for the valence electron, ΔE_3 and ΔE_4 are those for the core electrons, and ΔE_5 is the counterpotential vertex term of Fig. 4(d). Use of spectral representations for the electron propagators and the Feynman gauge matrix element allows a compact representation of the terms, specifically

$$\Delta E_{15} = -i\sum_{mn}\int\frac{dk_0}{2\pi}\,\frac{g_{vnmv}(k_0)\big[\sum_a g_{mana}(0) - U_{mn}\big]}{(\epsilon_v - k_0 - \epsilon_m)(\epsilon_v - k_0 - \epsilon_n)}, \quad (44)$$

$$\Delta E_{24} = -2i\sum_{amn}\int\frac{dk_0}{2\pi}\,\frac{g_{anmv}(k_0)g_{mvna}(\epsilon_{va})}{(\epsilon_a - k_0 - \epsilon_m)(\epsilon_v - k_0 - \epsilon_n)}, \quad (45)$$

$$\Delta E_3 = -i\sum_{amn}\int\frac{dk_0}{2\pi}\,\frac{g_{anma}(k_0)g_{mvnv}(0)}{(\epsilon_a - k_0 - \epsilon_m)(\epsilon_a - k_0 - \epsilon_n)}. \quad (46)$$

Here we have combined ΔE_1 and ΔE_5 into ΔE_{15}, and used $\Delta E_{24} = 2\Delta E_2 = 2\Delta E_4$. This sum-over-states form is useful for analysis of pole terms that come from a Wick rotation and the reference-state singularity. After the Wick rotation is carried out, an ultraviolet-divergent set of terms results, which we treat with differential equation techniques. We treat the ultraviolet divergence by adding and subtracting the same expression but with both electron propagators replaced with free propagators. Combining the subtracted term with the vertex makes the combination ultraviolet finite. The remaining term is evaluated in momentum space.

Care is required with the treatment of reference-state singularities, which we illustrate by considering ΔE_{24}. The summation over basis states is not defined when $m = a$ and $n = v$. However, after a Wick rotation, use of the energy shifts given in Eq. (28) gives the regulated expression

$$\Delta\tilde{E}_{24} = 2\sum_{abw}\int\frac{d\omega}{2\pi}\,\frac{g_{awbv}(i\omega)g_{bvwa}(\epsilon_{va})}{(i\omega + \epsilon_v\delta)^2}. \quad (47)$$

Here w and b are used to indicate that the magnetic quantum numbers of m and n are summed over. If one Taylor-expands $g_{awbv}(i\omega) = g_{awbv}(0) + |\omega|g'_{awbv}(0) + \cdots$, the higher-order terms are finite at $\omega = 0$ and the first term leads to a vanishing integral. The term linear in k_0 leads to an integral proportional to $\ln\delta$ multiplying $g'_{awbv}(0)$. A short analysis shows that this latter term reduces to the product of normalization integrals. The net result is that the δ behavior of this term is

$$\Delta E_{24} = \frac{2\alpha}{\pi}\ln\delta\sum_a g_{avva}(\epsilon_{va}). \quad (48)$$

One check of the calculation is varying δ and making sure this behavior was seen. The other was showing the independence of the complete calculation on this regulator. When these graphs are taken together the complete factor of E_{1F} is formed, which cancels the valence derivative term. The same thing happens for the core derivative terms.

We note in passing that while wave function renormalization and vertex renormalization counterterms are present, making the vertex diagram and the derivative terms ultraviolet finite, Ward's identity makes them cancel, and in our calculation we simply pull out the divergent terms from each diagram, which in dimensional regularization are terms that vary as $1/\delta$, and show that they cancel.

Turning to vacuum polarization, we note that our treatment in [26] was general, with care required only in using the factor $(2j_a + 1)$ in the core part of the perturbed orbital terms.

Finally, there is a set of two-loop diagrams collectively referred to as the two-loop Lamb shift. It has been calculated for the hydrogenic $1s$ ground state along with $2s$, $2p_{1/2}$, and $2p_{3/2}$ states [29], but is as yet not calculated for sodiumlike ions. Nevertheless, order-of-magnitude estimates based on the hydrogenic results with $1/n^3$ scaling and *ad hoc* screening corrections show that two-loop Lamb shifts are completely negligible for low- to mid-Z sodiumlike ions and only reach a few tens of meV at very high Z. In view of their small sizes and high uncertainties, we shall omit these corrections here and include their effects in our error estimates.

V. THREE-PHOTON EFFECTS

We have so far given a complete description of the contribution to energy levels of all Feynman diagrams involving one and two photons. Clearly the next logical step to take in the computational approach used here is to carry out a QED treatment of all diagrams involving three photons. As will be described further in the Conclusions, this is a large-scale task that has not yet been carried out. However, as mentioned above, second-order MBPT roughly reproduces the structure-related two-photon QED calculation. For this reason, to approximate three-photon effects we simply use third-order MBPT, including the dominant Coulomb correction along with a part of the Breit interaction terms, following the treatment of Ref. [11]. This ignores three-photon radiative corrections involving the one-, two-, and three-loop Lamb shift, which will again be discussed in the Conclusions. We present these results in the tables as $E3$, and note that they are relatively small.

VI. NUCLEAR CORRECTIONS

A. Nuclear structure effects

We have treated the nucleus as having infinite mass in the preceding discussion, but now take account of the finite mass. Before discussing the effect of nuclear recoil we mention three other nuclear effects that lie outside the scope of QED. While relatively small, each of these effects leads to some theoretical uncertainty, and this uncertainty will likely prove a fundamental barrier to progress in understanding the spectra of highly charged ions at some point.

The first uncertainty comes from the finite size of the nucleus and readily shows up in the lowest-order energy $E0$ calculated with a nuclear charge distribution modeled as a Fermi distribution,

$$\rho(r) = \frac{\rho_0}{1 + e^{4\ln 3(r-c)/t}}. \tag{49}$$

Here $t = 2.3$ fm and the parameter c is taken from Ref. [30]. At $Z = 74$ the value $c = 6.4464$ fm from that reference would have to change to 6.4458 fm to give the value from the more recent tabulation of Angeli and Marinova [31]. The change in the $3s$ energy would be 0.0024 eV, which is smaller than our theoretical uncertainty. With increasing experimental precision the need to know nuclear sizes accurately will eventually become important. This issue has received recent attention for the proton, where questions about its charge radius have been raised by experiments on muonic hydrogen [32]. More electron scattering data, new experiments on muonic atoms, and advances in nuclear structure theory are all called for to reduce this uncertainty. Alternatively one can assume QED is correct and use the spectra, as is done with hydrogen, to provide an independent method of determining the nuclear charge radius.

The second uncertainty is the distribution of nuclear magnetism, the Bohr-Weisskopf effect [33]. We have not included it in our treatment of the sodium isoelectronic sequence since it affects only hyperfine splittings and has very little effect on weight-averaged energy levels.

The last uncertainty comes from nuclear polarizability, another kind of two-photon exchange effect in which photons are exchanged between the valence electron and the nucleus. Part of this exchange is of course already accounted for in $E2$ when the nucleus remains in the ground state. When it is excited, a new effect called nuclear polarization is present. This effect can be significant for the actinides with low-lying nuclear excited states, particularly for the important case of uranium, where its contribution to the $2s$-$2p$ transition energies amounts to 0.03 eV [34]. However, with $1/n^3$ scaling and increased screening for sodiumlike ions, the effect on $n = 3$ states is likely to be just a few meV for uranium and can be ignored.

B. One-electron nuclear recoil

We now turn to the proper treatment of recoil effects, defined as terms suppressed by powers of m/M, with M the mass of the nucleus. While straightforward to include in the nonrelativistic case, in the relativistic case the problem is nontrivial even for one-electron ions. While the first proper treatments for the one-electron case were given long ago, it is only relatively recently that results valid to all orders in $Z\alpha$ have been presented, though only first order in m/M, in [35] and [36]. The second reference is valid only for a two-body system, as it employed a variant of the Bethe-Salpeter equation. An extremely compact re-derivation of the one-electron results also applicable to the many-electron case was presented by Shabaev in Ref. [37]. The remainder of this section presents his derivation using S-matrix techniques.

The simplest way to derive the leading effect of the finite mass of the nucleus can be made in the context of classical mechanics, where in a system with N_e light particles of mass m (the electrons) and a heavy particle of mass M (the nucleus), one considers the heavy particle's nonrelativistic kinetic energy

$$T_N = \frac{\vec{P}_N^2}{2M} \tag{50}$$

and evaluates it in the center-of-mass system. If one treats the electrons nonrelativistically, so that their kinetic energy is

$$T_e = \sum_{i=1}^{N_e} \frac{\vec{p}_i{}^2}{2m}, \tag{51}$$

eliminating T_N through

$$\vec{P}_N \to -\sum_{i=1}^{N_e} \vec{p}_i \tag{52}$$

turns $T_{\rm tot} = T_e + T_N$ into

$$T_{\rm tot} = \sum_{i=1}^{N_e} \frac{\vec{p}_i{}^2}{2m_r} + H_{\rm MP}, \tag{53}$$

where $m_r = m/(1 + m/M)$ is the reduced mass, and

$$H_{\rm MP} = \sum_{i\neq j} \frac{\vec{p}_i \cdot \vec{p}_j}{2M} \tag{54}$$

is the mass-polarization Hamiltonian. When this classical argument is extended to nonrelativistic quantum mechanics, it incorporates recoil exactly. As mentioned above, to treat the electrons relativistically, one cannot simply replace m with m_r in the Dirac equation, even for hydrogenlike atoms [38]. However, if one works in the approximation of keeping only m/M corrections, extending the classical argument described above to field theory, as shown by Shabaev in Ref. [37], allows recoil to be treated relativistically for both one- and many-electron systems. Before we reconsider this argument in the framework of our S-matrix approach, we note that terms of order $(m/M)^2$ would require a different treatment, as the kinetic energy of the nucleus would be more complicated. This problem has of course been solved for the two-particle case, most strikingly for positronium where there is no recoil expansion, through the use of the Bethe-Salpeter equation [39].

To generalize Eq. (52) to field theory, we first note that the electron momentum is now described as a single field operator,

$$\vec{p}_e = -i \int d^3x\, \psi^\dagger(x) \vec{\nabla} \psi(x). \tag{55}$$

Here the electron field operator $\psi(x) = \psi(\vec{x},t)$ is given by

$$\psi(x) = \sum_{n_p} \psi_{n_p}(\vec{x}) e^{-iE_{n_p}t} b_{n_p} + \sum_{n_m} \psi_{n_m}(\vec{x}) e^{-iE_{n_m}t} d^\dagger_{n_m}, \tag{56}$$

where n_p and n_m are positive and negative energy states, respectively, and normal ordering is implicit. The state ψ_{n_m} must be charge conjugated to describe positrons created by $d^\dagger_{n_m}$, but when they enter as intermediate sums, this step is not necessary. While there is also momentum carried by the electromagnetic field, we do not treat it here as it leads to m/M contributions suppressed by powers of α. However, the

electromagnetic field modifies the nuclear momentum in the usual way, with Eq. (50) now becoming

$$T_N \to \frac{|\vec{P}_N + Ze\vec{A}(\vec{0},t)|^2}{2M}. \tag{57}$$

The position of the nucleus is close to the origin, so $\vec{A}$ is evaluated there. Now using the field theory generalization of Eq. (52),

$$\vec{P}_N \to -\vec{p}_e, \tag{58}$$

we see that including the kinetic energy of the nucleus leads to three new operators to be added to $\tilde{H}_I$,

$$H_R = H_R(\mathrm{CC}) + H_R(\mathrm{CT}) + H_R(\mathrm{TT}), \tag{59}$$

with

$$H_R(\mathrm{CC}) = -\frac{1}{2M}\int d^3x \int d^3y\, \psi^\dagger(\vec{x},t) \times \vec{\nabla}_x\psi(\vec{x},t)\cdot\psi^\dagger(\vec{y},t)\vec{\nabla}_y\psi(\vec{y},t), \tag{60}$$

$$H_R(\mathrm{CT}) = \frac{iZe}{M}\,\vec{A}(\vec{0},t)\cdot\int d^3x\,\psi^\dagger(\vec{x},t)\vec{\nabla}_x\psi(\vec{x},t), \tag{61}$$

and

$$H_R(\mathrm{TT}) = \frac{Z^2e^2}{2M}\,\vec{A}(\vec{0},t)\cdot\vec{A}(\vec{0},t). \tag{62}$$

We note the similarity of $H_R(\mathrm{CC})$ with the Coulomb part of the QED Hamiltonian H_C when Coulomb gauge is used (as it is in this part of the calculation), where

$$H_C = e^2\int d^3x\int d^3y\,\frac{1}{|\vec{x}-\vec{y}|}\,\psi^\dagger(\vec{x},t)\psi(\vec{x},t)\psi^\dagger(\vec{y},t)\psi(\vec{y},t). \tag{63}$$

Both are instantaneous interactions, but a photon propagator is present in the latter.

We now have three new operators to add to $\tilde{H}_I$ in our S-matrix formulation, and treating them to first order will account for all m/M corrections. However, we are still dealing with a many-electron problem, so higher-order corrections from the nonrecoil parts of the interaction Hamiltonian will be present. A major advantage of this approach is that by choosing a realistic potential those higher-order corrections to an already small correction are negligible, as can be seen from Tables I and II for $Z = 74$.

We begin with $H_R(\mathrm{CC})$. While it is possible to express this in terms of an electron propagator, we carried out its analysis simply in terms of the field operators. For the one-electron case, where $|0_C\rangle = |0\rangle$, the true vacuum, the analysis leads to

$$\Delta E_{R1}(\mathrm{CC}) = \frac{1}{2M}\left(\sum_{n_p}\vec{p}_{vn_p}\cdot\vec{p}_{n_pv} - \sum_{n_m}\vec{p}_{vn_m}\cdot\vec{p}_{n_mv}\right). \tag{64}$$

An advantage of relativistic finite-basis-set methods is that they split naturally into positive and negative energy terms, making the evaluation of terms like $\Delta E_{R1}(\mathrm{CC})$ particularly straightforward.

We now continue to the transverse photon terms. In this case we must go beyond first-order perturbation theory and include the ordinary interaction with the photon field, which we refer to as H_T, either once or twice. We will encounter the transverse photon propagator, defined by

$$\begin{aligned} D_{ij}(\vec{x},x_0;\vec{y},y_0) &= -i\,\langle 0|T[A_i(\vec{x},x_0)A_j(\vec{y},y_0)]|0\rangle \\ &= \int\frac{dk_0}{2\pi}\,e^{-ik_0(x_0-y_0)}\int\frac{d^3k}{(2\pi)^3}\,e^{i\vec{k}\cdot(\vec{x}-\vec{y})}\,\frac{\delta_{ij}-\frac{k_ik_j}{\vec{k}^2}}{k_0^2-\vec{k}^2} \\ &\equiv \int\frac{dk_0}{2\pi}\,e^{-ik_0(x_0-y_0)}D_{ij}(\vec{x},\vec{y};k_0). \end{aligned} \tag{65}$$

To evaluate the effect of $H_R(\mathrm{CT})$, which has a single photon field, one interaction with H_T is required. We call this term $\Delta E_R(\mathrm{CT})$, given by the formula

$$\Delta E_R(\mathrm{CT}) = \frac{iZe}{2M}\sum_m\int d^3x\int d^3y\int\frac{dk_0}{2\pi}\,D_{ik}(\vec{x},\vec{0};k_0) \times\frac{\psi_v^\dagger(\vec{x})\alpha_i\psi_m(\vec{x})\,\psi_m^\dagger(\vec{y})\nabla_j\psi_v(\vec{y})}{k_0+\epsilon_v-\epsilon_m}. \tag{66}$$

Turning to $H_R(\mathrm{TT})$, we note that two factors of H_T are required by the presence of the two-photon fields. The formula for the associated energy shift is

$$\Delta E_R(\mathrm{TT}) = \frac{Z^2e^2}{2M}\sum_m\int d^3x\int d^3y\,D_{ik}(\vec{x},\vec{0};\omega)D_{jk}(\vec{y},\vec{0};\omega) \times\frac{\psi_v^\dagger(\vec{x})\alpha_i\psi_m(\vec{x})\,\psi_m^\dagger(\vec{y})\alpha_j\psi_v(\vec{y})}{k_0+\epsilon_v-\epsilon_m}. \tag{67}$$

Like the two-photon exchange diagrams, $\Delta E_R(CT)$ and $\Delta E_R(TT)$ are evaluated by carrying out a Wick rotation $k_0 \to i\omega$. As with those diagrams, this rotation passes poles, which lead to a set of easily evaluated terms.

We tabulate the sum of these recoil corrections, which agree well in the case of hydrogenlike ions with known results, as Recoil 1 in Tables I and II.

C. Two-electron nuclear recoil

When more than one electron is present, additional recoil corrections related to mass polarization are present. Leading two-electron recoil corrections are given by the generalized mass-polarization Hamiltonian

$$H_{\mathrm{MP}} = \frac{1}{2M}\sum_{i\neq j}\{\vec{p}_i\cdot\vec{p}_j + V(r_i)[\vec{\alpha}_i + (\vec{\alpha}_i\cdot\hat{r}_i)\hat{r}_i]\cdot\vec{p}_j\}, \tag{68}$$

where the second term in the summation is the relativistic correction to mass polarization [40] and has been shown to arise from the exchange of one transverse photon in a QED formalism [16]. Higher-order relativistic corrections from the exchange of two transverse photons have been calculated for lithiumlike ions [16]. They are negligibly small at low Z but are significant at high Z as they increase very rapidly along the isoelectronic sequence. However, as pointed out in [15], these corrections are well approximated by the expectation values of the operator $\frac{1}{2M}\sum_{i\neq j}\vec{q}_i\cdot\vec{q}_j$ where

$$\vec{q}_i = \tfrac{1}{2}\,V(r_i)[\vec{\alpha}_i + (\vec{\alpha}_i\cdot\hat{r}_i)\,\hat{r}_i]. \tag{69}$$

TABLE III. Breakdown of structure and QED contributions to the ionization potentials (a.u.) of the $n = 3$ states for selected sodiumlike ions using the Kohn-Sham potential.

Terms	$Z = 30$	$Z = 40$	$Z = 50$	$Z = 60$	$Z = 70$	$Z = 83$	$Z = 92$
				$3s_{1/2}$			
$E0$	−26.32286	−57.07157	−100.1534	−156.4747	−227.3405	−344.3878	−444.9521
$E1$	−0.76169	−1.07398	−1.3790	−1.6751	−1.9593	−2.3037	−2.5180
$E2$	−0.01956	−0.02364	−0.0285	−0.0346	−0.0423	−0.0560	−0.0687
$E3$	0.00060	0.00056	0.0005	0.0005	0.0004	0.0005	0.0005
Recoil 1	0.00025	0.00038	0.0005	0.0007	0.0008	0.0012	0.0014
Recoil 2	−0.00003	−0.00004	−0.0001	−0.0001	−0.0001	−0.0001	−0.0002
SE	0.00625	0.01991	0.0479	0.0987	0.1844	0.3814	0.6101
Uehling	−0.00054	−0.00206	−0.0059	−0.0142	−0.0312	−0.0806	−0.1519
WK	0.00000	0.00003	0.0001	0.0004	0.0010	0.0035	0.0075
SE screen	−0.00131	−0.00212	−0.0035	−0.0057	−0.0091	−0.0167	−0.0257
VP screen	0.00005	0.00014	0.0003	0.0007	0.0014	0.0032	0.0059
Sum	−27.09884	−58.15238	−101.5209	−158.1034	−229.1944	−346.4552	−447.0911
				$3p_{1/2}$			
$E0$	−24.81041	−54.77595	−97.0181	−152.4192	−222.2571	−337.7626	−437.1343
$E1$	−0.68279	−0.93787	−1.1671	−1.3603	−1.5034	−1.5800	−1.5251
$E2$	−0.02424	−0.03049	−0.0376	−0.0466	−0.0582	−0.0790	−0.0989
$E3$	0.00067	0.00066	0.0006	0.0006	0.0006	0.0006	0.0007
Recoil 1	0.00024	0.00037	0.0005	0.0006	0.0007	0.0010	0.0011
Recoil 2	−0.00013	−0.00020	−0.0003	−0.0003	−0.0004	−0.0004	−0.0005
SE	−0.00015	−0.00023	0.0004	0.0033	0.0120	0.0449	0.0994
Uehling	0.00000	−0.00004	−0.0002	−0.0009	−0.0028	−0.0115	−0.0286
WK	0.00000	0.00000	0.0000	0.0000	0.0001	0.0007	0.0020
SE screen	−0.00079	−0.00140	−0.0026	−0.0045	−0.0077	−0.0156	−0.0258
VP screen	0.00004	0.00013	0.0003	0.0006	0.0013	0.0032	0.0061
Sum	−25.51756	−55.74501	−98.2241	−153.8266	−223.8148	−339.3987	−438.7039
				$3p_{3/2}$			
$E0$	−24.60326	−53.96151	−94.7313	−147.1273	−211.4351	−313.4420	−396.7226
$E1$	−0.69489	−0.97285	−1.2461	−1.5159	−1.7850	−2.1438	−2.4103
$E2$	−0.02349	−0.02886	−0.0345	−0.0410	−0.0484	−0.0598	−0.0687
$E3$	0.00064	0.00062	0.0006	0.0005	0.0005	0.0004	0.0004
Recoil 1	0.00024	0.00036	0.0005	0.0006	0.0007	0.0009	0.0010
Recoil 2	−0.00013	−0.00019	−0.0003	−0.0003	−0.0004	−0.0004	−0.0004
SE	0.00027	0.00125	0.0040	0.0101	0.0220	0.0521	0.0879
Uehling	0.00000	0.00000	0.0000	−0.0001	−0.0002	−0.0006	−0.0012
WK	0.00000	0.00000	0.0000	0.0000	0.0000	0.0001	0.0002
SE screen	−0.00094	−0.00156	−0.0026	−0.0042	−0.0066	−0.0113	−0.0161
VP screen	0.00004	0.00011	0.0003	0.0005	0.0009	0.0019	0.0032
Sum	−25.32152	−54.96262	−96.0095	−148.6771	−213.2515	−315.6024	−399.1266

As a result, two-electron recoil corrections for many-electron systems are closely given by the relativistic mass-polarization Hamiltonian

$$H_{\rm MP}^{\rm rel} = \frac{1}{2M}\sum_{i\neq j}(\vec{p}_i + \vec{q}_i)\cdot(\vec{p}_j + \vec{q}_j), \tag{70}$$

and results for sodiumlike ions thus calculated are listed as Recoil 2 in Tables I and II.

VII. APPLICATION TO THE SODIUM ISOELECTRONIC SEQUENCE

In addition to the Kohn-Sham results for $Z = 74$ in Table II, structure and QED contributions to the ionization potentials of the $3s$ and $3p$ states as calculated with the same potentials are shown for a few more selected sodiumlike ions in Table III. The nonrelativistic $1/Z$-expansion behavior of the structure terms is apparent here, along with the effect of the relativistic $Z\alpha$ expansion [41] as is evidenced by the slowly varying, nonconstant $E2$ term. While the recoil corrections are seen to go up slowly with Z, QED corrections are definitely increasing very rapidly along the isoelectronic sequence.

In Table IV, total ionization potential and transition energy results are given for ions with $Z = 30$–100, along with the root-mean-square nuclear charge radii $R_{\rm rms}$ as derived from the Fermi c and t parameters which, as mentioned at the beginning of the previous section, are used to model the nuclear potentials here. The same nuclear parameters are used in our earlier work for lithiumlike ions [15]. Nuclear finite-size corrections are small corrections, and uncertainties in $R_{\rm rms}$ have very little effects on most contributions to the ionization energy except

TABLE IV. Root-mean-square nuclear radius R_{rms} (fm), $3s$, $3p_{1/2}$, and $3p_{3/2}$ ionization potentials (a.u.), and $3s$-$3p$ transition energies $\Delta 3p$ (eV) for sodiumlike ions.

Z	$R_{\rm rms}$	$3s$	$3p_{1/2}$	$3p_{3/2}$	$\Delta 3p_{1/2}$	$\Delta 3p_{3/2}$	Z	R_{rms}	$3s$	$3p_{1/2}$	$3p_{3/2}$	$\Delta 3p_{1/2}$	$\Delta 3p_{3/2}$
30	3.955	−27.0988	−25.5176	−25.3215	43.029	48.363	66	5.083	−198.914	−193.992	−185.972	133.92	352.17
31	3.998	−29.6691	−28.0074	−27.7770	45.218	51.487	67	5.210	−206.246	−201.213	−192.609	136.96	371.08
32	4.079	−32.3569	−30.6143	−30.3452	47.418	54.741	68	5.123	−213.737	−208.589	−199.368	140.08	391.00
33	4.104	−35.1626	−33.3387	−33.0262	49.631	58.135	69	5.192	−221.385	−216.122	−206.249	143.21	411.88
34	4.171	−38.0867	−36.1811	−35.8200	51.856	61.679	70	5.237	−229.194	−223.815	−213.252	146.38	433.83
35	4.156	−41.1299	−39.1420	−38.7270	54.094	65.387	71	5.246	−237.167	−231.669	−220.377	149.61	456.88
36	4.230	−44.2927	−42.2220	−41.7471	56.346	69.268	72	5.290	−245.304	−239.686	−227.626	152.88	481.07
37	4.245	−47.5757	−45.4217	−44.8806	58.613	73.337	73	5.299	−253.610	−247.870	−234.998	156.19	506.47
38	4.242	−50.9795	−48.7417	−48.1276	60.895	77.606	74	5.359	−262.084	−256.221	−242.493	159.54	533.10
39	4.244	−54.5049	−52.1825	−51.4882	63.193	82.088	75	5.351	−270.732	−264.744	−250.113	162.96	561.07
40	4.273	−58.1524	−55.7450	−54.9626	65.508	86.798	76	5.376	−279.555	−273.439	−257.858	166.42	590.40
41	4.318	−61.9228	−59.4298	−58.5511	67.839	91.750	77	5.401	−288.555	−282.311	−265.728	169.92	621.16
42	4.415	−65.8169	−63.2375	−62.2537	70.188	96.960	78	5.418	−297.736	−291.361	−273.724	173.48	653.41
43	4.410	−69.8354	−67.1690	−66.0707	72.556	102.44	79	5.437	−307.101	−300.593	−281.845	177.09	687.23
44	4.475	−73.9791	−71.2250	−70.0022	74.943	108.22	80	5.475	−316.651	−310.009	−290.094	180.73	722.67
45	4.502	−78.2490	−75.4064	−74.0486	77.350	114.30	81	5.483	−326.392	−319.614	−298.469	184.45	759.83
46	4.526	−82.6457	−79.7140	−78.2099	79.778	120.71	82	5.505	−336.326	−329.409	−306.972	188.21	798.76
47	4.542	−87.1704	−84.1486	−82.4864	82.227	127.46	83	5.531	−346.455	−339.399	−315.602	192.02	839.55
48	4.613	−91.8238	−88.7112	−86.8784	84.698	134.57	84	5.539	−356.785	−349.586	−324.362	195.89	882.30
49	4.619	−96.6069	−93.4027	−91.3860	87.192	142.07	85	5.578	−367.318	−359.976	−333.250	199.79	927.04
50	4.655	−101.521	−98.2241	−96.0095	89.710	149.97	86	5.632	−378.058	−370.571	−342.268	203.72	973.89
51	4.704	−106.567	−103.176	−100.749	92.252	158.30	87	5.640	−389.011	−381.376	−351.416	207.75	1023.01
52	4.804	−111.745	−108.261	−105.605	94.818	167.08	88	5.663	−400.179	−392.395	−360.694	211.80	1074.43
53	4.752	−117.058	−113.478	−110.578	97.414	176.33	89	5.670	−411.568	−403.633	−370.104	215.93	1128.29
54	4.826	−122.506	−118.830	−115.668	100.03	186.08	90	5.804	−423.174	−415.093	−379.646	219.88	1184.45
55	4.807	−128.090	−124.317	−120.875	102.68	196.35	91	5.700	−435.025	−426.783	−389.320	224.29	1243.72
56	4.840	−133.812	−129.940	−126.199	105.36	207.17	92	5.861	−447.091	−438.704	−399.127	228.23	1305.18
57	4.855	−139.673	−135.702	−131.641	108.07	218.57	93	5.744	−459.420	−450.866	−409.067	232.78	1370.20
58	4.877	−145.674	−141.602	−137.201	110.81	230.57	94	5.794	−471.980	−463.271	−419.141	236.99	1437.83
59	4.893	−151.817	−147.644	−142.880	113.58	243.20	95	5.787	−484.798	−475.928	−429.350	241.36	1508.80
60	4.915	−158.103	−153.827	−148.677	116.38	256.50	96	5.816	−497.868	−488.840	−439.695	245.65	1582.97
61	4.962	−164.534	−160.153	−154.593	119.21	270.50	97	5.816	−511.206	−502.017	−450.175	250.04	1660.72
62	5.031	−171.111	−166.625	−160.629	122.08	285.23	98	5.844	−524.810	−515.463	−460.792	254.32	1742.00
63	5.041	−177.836	−173.243	−166.784	124.98	300.72	99	5.865	−538.692	−529.188	−471.547	258.61	1827.11
64	5.089	−184.710	−180.009	−173.060	127.92	317.01	100	5.886	−552.858	−543.199	−482.439	262.85	1916.20
65	5.099	−191.735	−186.925	−179.455	130.90	334.15							

the one-electron eigenenergy $E0$. Indeed, it has been shown that different choices of $R_{\rm rms}$ can lead to fractions of an eV changes in the $2s$-$2p$ transition energies for mid- to high-Z lithiumlike ions, with up to 0.7 eV change for lithiumlike thorium ($Z = 90$), and that these changes are largely due to differences in the $2s$ eigenenergies, and to a lesser extend the $2p$ eigenenergies [15]. For the $n = 3$ states of sodiumlike ions considered here, uncertainties in the finite nuclear size corrections are less significant due to the $1/n^3$ scaling, and as in the case of lithiumlike ions, can easily be corrected by recalculating the $3s$ and $3p$ eigenenergies $E0$ with more reliable nuclear charge radii.

In Table V, the present $3s$-$3p$ transition energies are compared with experiment and with other theories. Uncertainties in the present results at low Z are due mainly to the incomplete treatment of higher-order correlation corrections in evaluating the $E3$ term. At high Z, they are dominated by the omission of two-loop Lamb shifts. Experimental results listed in Table V are from NIST's online database of atomic spectra [42] at low to mid Z and from electron-beam ion-trap (EBIT) measurements at high Z [20,21,43]. On the theory side, high-precision results are available for selected ions from the relativistic MBPT (RMBPT) calculations of Blundell [14] who evaluated all screened QED corrections in Figs. 2 and 4 except the vertex exchange terms in Fig. 4(d), which were deemed to be very small and were neglected. There are also relativistic configuration-interaction (RCI) results for $Z = 74$ [20,44] and 92 [43] which include directly calculated QED energies, although QED screening and relaxation effects are only approximately accounted for by evaluating the one-loop diagrams in Fig. 2 with Kohn-Sham wave functions specific to the initial and final states. By far the most complete theoretical tabulation of these energies is by Kim *et al.* [13]. It is based on multiconfiguration Dirac-Fock (MCDF) calculations with correlation energies derived from RMBPT and the resulting structure energies are thus essentially the same as the RMBPT energies of Refs. [11] and [14]. However, as QED corrections are calculated with the *ad hoc* Welton's method [45] and are

TABLE V. The $3s$-$3p$ transition energies (eV) of sodiumlike ions. RMBPT results are from [14]. Unless otherwise specified, experimental results are from the NIST Atomic Spectra Database [42].

	$3s$-$3p_{1/2}$			$3s$-$3p_{3/2}$			
Z	Present	RMBPT	Expt.	Present	RMBPT	RCI	Expt.
30	43.029(2)	43.025(1)	43.023	48.363(2)	48.362(1)		48.361
31	45.218(2)		45.212	51.487(2)			51.485
32	47.418(2)		47.412	54.741(2)			54.739
33	49.631(2)		49.630	58.135(2)			58.135
34	51.856(2)		51.826	61.679(2)			61.662
35	54.094(2)		54.090	65.387(2)			65.386
36	56.346(2)		56.340	69.268(2)			69.267
37	58.613(2)		58.607	73.337(2)			73.337
38	60.895(2)		60.877	77.606(2)			77.597
40	65.508(2)	65.503(2)		86.798(2)	86.795(2)		
42	70.188(2)		70.187	96.960(2)			96.963
50	89.710(1)	89.710		149.97(1)	149.97		
54	100.03		100.05	186.08			186.13
55	102.68		102.73	196.35			196.38
56	105.36		105.39	207.17			207.24
64	127.92(1)	127.94(1)		317.01(1)	317.07(1)		
72	152.88(2)		152.91(2)[a]	481.07(2)			481.14(31)[a]
73	156.19(2)		156.19(2)[a]	506.47(2)			506.14(37)[a]
74	159.54(2)		159.57(2)[a]	533.10(2)		533.09(5)[b]	533.20(11)[c]
							533.43(38)[a]
78	173.48(3)	173.51(1)		653.41(2)	653.41(1)		
79	177.09(3)		177.14(3)[a]	687.23(3)			686.28(83)[a]
80	180.73(3)	180.78(2)		722.67(3)	722.67(1)		
82	188.21(3)	188.27(2)		798.76(3)	798.76(1)		
90	219.88(5)	219.98(2)		1184.45(5)	1184.44(1)		
92				1305.18(5)		1305.11(7)[d]	1305.12(2)[d]

[a]Reference [21].
[b]Reference [44].
[c]Reference [20].
[d]Reference [43].

rather crude, these transition energy results are not included in the present comparisons.

As shown in Table V, agreements between theory and experiment are generally very good. This is further illustrated in Figs. 5 and 6 for the $3s$-$3p_{1/2}$ and $3s$-$3p_{3/2}$ transitions, respectively, where discrepancies are seen to be mostly within 0.1 eV even at high Z. In spite of the close agreements, the $3s$-$3p_{1/2}$ RMBPT energies in Fig. 5 can be seen to deviate more and more from the present results as Z increases, and these discrepancies arise mainly from the structure energy differences. The same trend has also been observed in the $2s$-$2p_{1/2}$ structure energy differences between RMBPT and our S-matrix calculations for lithiumlike ions [15] and underscores the importance of the correct treatment of frequency-dependent Breit interactions and ladder and cross-ladder correlation diagrams in Figs. 3(d) and 3(e). It is interesting to note that the experimental results of Gillaspy *et al.* at $Z = 72$–79 [21] appear to track the RMBPT results closely, though they are also consistent with the present results, which have comparable uncertainties of about 0.02–0.03 eV in this Z range.

In Fig. 6, it can be seen that the present $3s$-$3p_{3/2}$ transition energies are in good agreements with RMBPT results [14] along the isoelectronic sequence and with RCI results at $Z = 74$ and 92 [20,43,44]. While this is due in part to cancellations of errors between the structure and QED energies, neither of these differences is too much larger. With

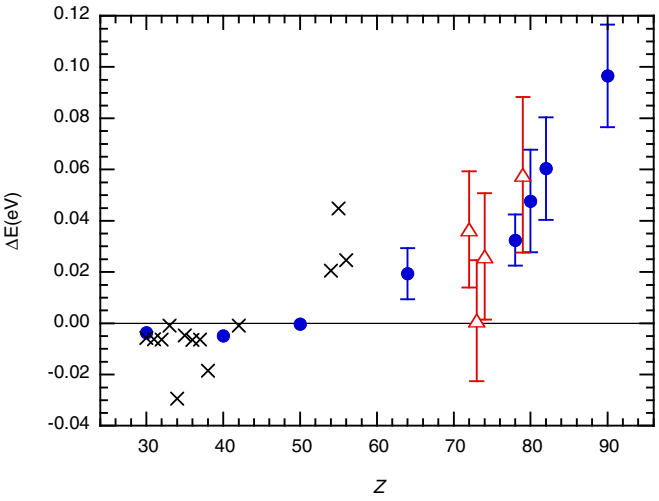

FIG. 5. (Color online) Experimental and theoretical energies relative to the present results for the $3s$-$3p_{1/2}$ transition. Solid circles, RMBPT [14]; crosses, NIST [42]; open triangles, Gillaspy *et al.* [21].

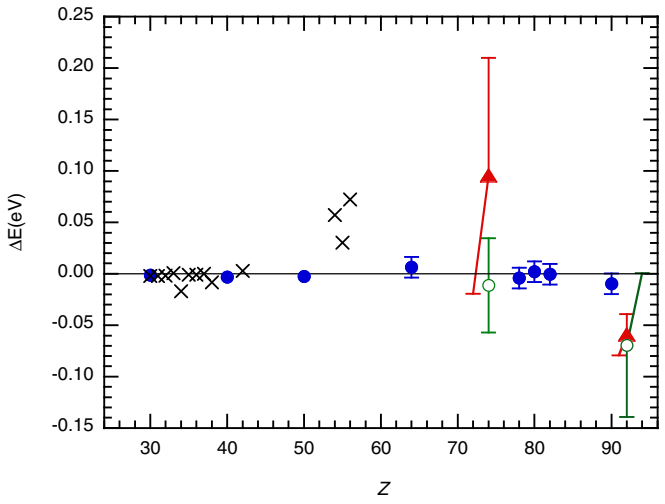

FIG. 6. (Color online) Experimental and theoretical energies relative to the present results for the $3s$-$3p_{3/2}$ transition. Solid circles, RMBPT [14]; open circles, RCI [20,43]; crosses, NIST [42]; closed triangles, EBIT [20,43].

the estimated uncertainties of 0.02 and 0.05 eV at $Z = 74$ and 92, respectively, the present results are also in good agreement with the EBIT measurements [20,43]. Not shown here are the measurements of Gillaspy *et al.* [21] which are listed in Table V but are mostly outside the range of this figure. Those results are nevertheless consistent with the present ones as they have relatively large uncertainties.

VIII. CONCLUSIONS

One of the best-known successes of QED is the accurate theoretical prediction of the anomalous magnetic moment of the electron, made possible by the smallness of the expansion parameter α/π in the formula

$$a_e = \sum_{i=1} C_i \left(\frac{\alpha}{\pi}\right)^i. \tag{71}$$

The constants C_i are now known up to $i = 5$ [46], and are all of order 1. Because α/π is about two parts per thousand, the theoretical uncertainty is now well under the part per trillion level. The calculation of a_e is the best example of precision calculation in physics. Another example of the theory working with extremely high accuracy is the determination of the electron mass through study of the g factors of hydrogenic ions [47]. Given these successes, and the fact that the electromagnetic interaction is the dominant force in all of atomic physics and chemistry, it is natural to ask if the successful application of QED to the electron anomalous magnetic moment can be extended to many-electron systems. However, a diagrammatic approach to problems with more than one electron generally fails, as the interaction between electrons cannot be treated perturbatively. An exception to this case, which we have concentrated on in this paper, is in highly charged ions, where the attraction to the nucleus is much larger than the electron-electron interaction. This allows one to expand in powers of both $1/Z$ and α, which leads to rapid convergence providing one avoids expanding in $Z\alpha$.

The isoelectronic sequences amenable to treatment with the methods described in this paper include all alkali metals, and also any ion with a single electron outside closed shells. An important example of the latter case is the copper isoelectronic sequence, where measurements on many ions have been carried out, some with very high accuracy. An alkali metal of particular interest that has been relatively unstudied is potassium. The ground state of potassiumlike ions is $3d_{3/2}$. The $3d$ fine structure of these ions is almost totally free of nuclear size uncertainty, and in the range $Z = 27$–33 the transition lies in the optical range and could be measured in principle with extremely high accuracy, as the ground state has zero width and the $3d_{5/2}$ state is very narrow. This then could be used to provide an independent determination of α, with the precision almost certainly limited by theory. Many terms, however, cancel out when dealing with fine structure, as was illustrated in Ref. [48]. With 19 electrons, variational methods are impractical, so the approach given here seems the most promising.

In order to extend this work to more sequences one must change the starting point from $a_v^\dagger|0_C\rangle$ to that appropriate for the sequence in question. An obvious sequence to be considered is the helium isoelectronic sequence, which has recently been measured [49] to have a spectrum possibly in disagreement with theory [50]. Our approach is at present limited to states that do not have significant configuration mixing, a disadvantage of the S-matrix formalism. Specifically, as the $2p_{1/2}$ and $2p_{3/2}$ states have different energies, $1s2p_{1/2}$ and $1s2p_{3/2}$ $J = 1$ configurations cannot be mixed to form starting states for perturbation calculations. While states without mixing do not have this problem, and a QED treatment of the ladder and crossed-ladder diagrams has been given for the $1s2p_{1/2}\,{}^3P_0$ and $1s2p_{3/2}\,{}^3P_2$ states in Ref. [28], most experiments involve the strongly mixed $1s2p\,{}^{1,3}P_1$ states, so progress in this direction with our methods awaits the overcoming of the difficulty just mentioned. The same comment applies to the fairly wide range of systems which can be described with a particle-hole approach [51]. Excited states of the noble gases, in particular, have many excitations where a core electron is excited to a valence state, with the starting point being

$$F_{av} a_a a_v^\dagger |0_C\rangle, \tag{72}$$

where F_{av} is an angular decoupling factor. However, the case with one electron outside a closed shell remains the simplest many-body problem to study, and we return to discussion of that case.

We have presented results only for at least 19-times-ionized sodiumlike ions. Were we to use the Kohn-Sham potential on neutral sodium, QED effects such as the Lamb shift would be much smaller than the discrepancy between MBPT taken through third order and experiment, which is over 1% for the $3s$ removal energy. While the Lamb shift has been evaluated for neutral sodium [52,53], it depends on the potential used. Its size, however, is of order 12 μhartrees. We consider it an outstanding challenge to methods of solving the Schrödinger equation to reach the μhartree level, so that the actual value of the Lamb shift could be reliably inferred through the disagreement between theory and experiment.

We turn finally to the issue of QED in the context of highly charged ions. Assuming that structure has been solved to a

certain accuracy, one then wishes to calculate QED effects to at least the same accuracy. Provided that nuclear uncertainties can be controlled, the systematic evaluation of all three-photon diagrams in a completely field-theoretic manner is clearly the obvious next step. When all three photons are exchanged between electrons, it should be possible to show that the result presented here, $E3$, is recovered along with QED corrections, just as was done for two-photon exchange in this paper. These QED corrections are at the forefront of one-electron QED bound-state calculations, and should enter at the α^3 a.u. level. There are many diagrams involving three photons, the three-loop Lamb shift, entering at order $Z^4\alpha^5$, one-photon exchange corrections to the two-loop Lamb shift at $Z^3\alpha^4$, and two-photon exchange corrections to the one-loop Lamb shift at $Z^2\alpha^3$. Comparing these scalings to the basic order of the energy level of an ion, Z^2, we see that all are quite small, but important at the ppm level.

In conclusion, we have generalized methods used in the lithium isoelectronic sequence to many-electron alkali-metal sequences. These methods have been applied to sodiumlike ions and good agreement with experiment and other calculations found. Theoretical progress will involve a complete evaluation of the three-photon diagrams along with improvement in the accurate solution of the many-body problem.

ACKNOWLEDGMENTS

We thank Vladimir Shabaev and Steve Blundell for useful discussions and Greg Adkins for a reading of the manuscript. The work of J.S. was supported in part by NSF Grant No. PHY-1068065. The work of K.T.C. was performed under the auspices of the U.S. Department of Energy by Lawrence Livermore National Laboratory under Contract No. DE-AC52-07NA27344.

[1] P. J. Mohr, B. N. Taylor, and D. B. Newell, Rev. Mod. Phys. **84**, 1527 (2012).
[2] W. H. Furry, Phys. Rev. **81**, 115 (1951).
[3] Ulrich D. Jentschura, Peter J. Mohr, and Gerhard Soff, Phys. Rev. A **63**, 042512 (2001).
[4] W. E. Caswell and G. P. Lepage, Phys. Lett. B **167**, 437 (1986).
[5] C. Schwartz, Int. J. Mod. Phys. E **15**, 877 (2006).
[6] K. Pachucki and V. Yerokhin, Can. J. Phys. **89**, 95 (2011).
[7] K. Piszczatowsi, G. Lach, M. Przybytek, J. Komasa, K. Pachucki, and B. Jeziorsi, J. Chem. Theory Comput. **5**, 3039 (2009).
[8] G. E. Brown and D. G. Ravenhall, Proc. R. Soc. London, Ser. A **208**, 552 (1951).
[9] J. Sucher, Int. J. Quantum Chem. **25**, 3 (1984).
[10] W. R. Johnson, S. A. Blundell, and J. Sapirstein, Phys. Rev. A **37**, 2764 (1988).
[11] W. R. Johnson, S. A. Blundell, and J. Sapirstein, Phys. Rev. A **38**, 2699 (1988).
[12] W. R. Johnson, S. A. Blundell, and J. Sapirstein, Phys. Rev. A **42**, 1087 (1990).
[13] Y.-K. Kim, D. H. Baik, P. Indelicato, and J. P. Desclaux, Phys. Rev. A **44**, 148 (1991).
[14] S. A. Blundell, Phys. Rev. A **47**, 1790 (1993).
[15] J. Sapirstein and K. T. Cheng, Phys. Rev. A **83**, 012504 (2011).
[16] A. N. Artemyev, V. M. Shabaev, and V. A. Yerokhin, Phys. Rev. A **52**, 1884 (1995).
[17] I. Lindgren, *Relativistic Many-Body Theory: A New Field-Theoretical Approach* (Springer, New York, 2011).
[18] V. M. Shabaev, Phys. Rep. **356**, 119 (2002).
[19] H. J. Monkhorst, Int. J. Quantum Chem. **12**, 421 (1977).
[20] J. Clementson and P. Beiersdorfer, Phys. Rev. A **81**, 052509 (2010).
[21] J. D. Gillaspy, I. N. Draganic, Yu. Ralchenko, J. Reader, J. N. Tan, J. M. Pomeroy, and S. M. Brewer, Phys. Rev. A **80**, 010501(R) (2009).
[22] R. Cowan, *The Theory of Atomic Spectra* (University of California Press, Berkeley, CA, 1981), Chap. 7, Secs. 7–11.
[23] J. Sapirstein and K. T. Cheng, Phys. Rev. A **64**, 022502 (2001).
[24] J. Sucher, Phys. Rev. **107**, 1448 (1957).
[25] K. T. Cheng, W. R. Johnson, and J. Sapirstein, Phys. Rev. A **47**, 1817 (1993).
[26] J. Sapirstein and K. T. Cheng, Phys. Rev. A **68**, 042111 (2003).
[27] W. R. Johnson, S. A. Blundell, and J. Sapirstein, Phys. Rev. A **37**, 307 (1988).
[28] P. J. Mohr and J. Sapirstein, Phys. Rev. A **62**, 052501 (2000).
[29] V. A. Yerokhin, Phys. Rev. A **80**, 040501(R) (2009); V. A. Yerokhin, P. Indelicato, and V. M. Shabaev, Phys. Rev. Lett. **97**, 253004 (2006).
[30] W. R. Johnson and G. Soff, At. Data Nuc. Data Tables **33**, 405 (1985). For $Z = 90$ and $Z = 92$ we use $c = 7.0598$ and $c = 7.137\,53$ fm, respectively, as derived from measurements by Zumbro *et al.*, Phys. Lett. B **167**, 383 (1986); J. D. Zumbro, E. B. Shera, Y. Tanaka, C. E. Bemis, R. A. Naumann, M. V. Hoehn, W. Reuter, and R. M. Steffen, Phys. Rev. Lett. **53**, 1888 (1984).
[31] I. Angeli and K. P. Marinova, At. Data Nucl. Data Tables **99**, 69 (2013).
[32] R. Pohl *et al.*, Nature (London) **466**, 213 (2010).
[33] A. Bohr and V. Weisskopf, Phys. Rev. **77**, 94 (1950).
[34] G. Plunien and G. Soff, Phys. Rev. A **51**, 1119 (1995). Due to a mistake in the formulas, results of this work are too large by a factor of 2π as pointed out in the Erratum: **53**, 4614(E) (1996).
[35] A. N. Artemyev, V. M. Shabaev, and V. A. Yerokhin, J. Phys. B **28**, 5201 (1995). Note that these calculations are based on formulas derived much earlier by V. M. Shabaev, Teor. Mat. Fiz. **64**, 413 (1973) [Sov. Phys. JETP **37**, 211 (1973)].
[36] G. S. Adkins, S. Morrison, and J. Sapirstein, Phys. Rev. A **76**, 042508 (2007).
[37] V. M. Shabaev, Phys. Rev. A **57**, 59 (1998).
[38] W. A. Barker and F. N. Glover, Phys. Rev. **99**, 317 (1955).
[39] Thomas Fulton and Paul C. Martin, Phys. Rev. **95**, 811 (1954).
[40] C. W. P. Palmer, J. Phys. B **20**, 5987 (1987); A. P. Stone, Proc. Phys. Soc. **77**, 786 (1961); **81**, 868 (1963).
[41] H. Doyle, Adv. At. Mol. Phys. **5**, 337 (1969).
[42] NIST Atomic Spectra Database, http://physics.nist.gov/PhysRefData/ASD
[43] M. H. Chen, K. T. Cheng, P. Beiersdorfer, and J. Sapirstein, Phys. Rev. A **68**, 022507 (2003).
[44] M. H. Chen and K. T. Cheng, Phys. Rev. A **84**, 012513 (2011).

[45] T. A. Welton, Phys. Rev. **74**, 1157 (1948).
[46] T. Aoyama, M. Hayakawa, T. Kinoshita, and M. Nio, Phys. Rev. Lett. **109**, 111807 (2012).
[47] V. A. Yerokhin and Z. Harman, Phys. Rev. A **88**, 042502 (2013).
[48] J. Sapirstein and K. T. Cheng, Phys. Rev. A **73**, 012503 (2006).
[49] C. T. Chantler, M. N. Kinnane, J. D. Gillaspy, L. T. Hudson, A. T. Payne, L. F. Smale, A. Henins, J. M. Pomeroy, J. N. Tan, J. A. Kimpton, E. Takacs, and K. Makonyi, Phys. Rev. Lett. **109**, 153001 (2012).
[50] A. N. Artemyev, V. M. Shabaev, V. A. Yerokhin, G. Plunien, and G. Soff, Phys. Rev. A **71**, 062104 (2005).
[51] E. Avgoustoglou, W. R. Johnson, D. R. Plante, J. Sapirstein, S. Sheinerman, and S. A. Blundell, Phys. Rev. A **46**, 5478 (1992).
[52] J. Sapirstein and K. T. Cheng, Phys. Rev. A **66**, 042501 (2002).
[53] V. M. Shabaev, I. I. Tupitsyn, and V. A. Yerokhin, Phys. Rev. A **88**, 012513 (2013).